

Particle Tracking and Multispectral Collocation Method for Particle-to-Particle Binding Assays

Supporting Information

*Anita Rogacs, Juan G. Santiago**

Department of Mechanical Engineering, Stanford University, Stanford, California, 94305

*To whom correspondence should be addressed. E-mail: juan.santiago@stanford.edu. Fax: 650-723-7657

This document contains the following supplementary figures and information further describing our particle collocation method:

- Section S.1. List of symbols
- Section S.2. PITC algorithm
- Section S.3. Effective diffusivity of a particle pair
- Section S.4. 2D nearest neighbor model for randomly distributed particles
- Section S.5: Influence of image SNR and particle density on particle tracking accuracy
- Section S.6. Limit of detection of PITC method
- Section S.7: Influence of particle density on collocation performance
- Section S.8: DNA induced bead-to-bead binding assay
- Section S.9: List of fluorescent beads and DNA sequences
- Section S.10: Chip schematic and loading protocol

Section S.1. List of symbols

$\Delta i, \Delta j$	Image displacement (x,y)
α	Angular displacement
r_p	Physical particle radius
r_{pi}	Particle image radius
D_p	Diffusivity of particle, p ($\text{m}\cdot\text{s}^{-2}$)
D_{eff}	Effective diffusivity of a pair of particles ($\text{m}\cdot\text{s}^{-2}$)
w	Particle probability distribution
η	Particle density (m^{-2})
L_{IP}	Mean inter-particle distance in 2-D (m)
L_{ch}	Characteristic minimum particle center-to-center distance in object space
x_o	x-coordinate of particle mask
x_p	x-coordinate of particle, p
y_o	y-coordinate of particle mask
y_p	y-coordinate of particle, p
A	Peak fluorescence amplitude of particle image
b	Local background image intensity
σ_m	Characteristic size of particle brightness pattern of PMC mask
l_p	Pixel dimension in object space
g	Number of ‘unity’ pixels for a particle group in the binarized image
I_P	Fluorescence intensity of particle image
I_p	Integrated fluorescence intensity of background corrected particle image
I_m	Peak fluorescence intensity of particle mask
I_{raw}	Raw particle image fluorescence intensity
I_{bg}	Background fluorescence intensity
I_{flat}	Flatfield fluorescence intensity
I_c	Corrected particle image fluorescence intensity
v_{diff}	Diffusive particle velocity ($\text{m}\cdot\text{s}^{-1}$)
$\bar{v}_{p,x}$	Uniform advective particle velocity in MC simulation ($\text{m}\cdot\text{s}^{-1}$)
$\bar{v}_{p,a}$	Apparent particle velocity ($\text{m}\cdot\text{s}^{-1}$)
\bar{v}_{PIV}	Predicted particle velocity from PIV measurements ($\text{m}\cdot\text{s}^{-1}$)
t_m	Length of particle monitoring time
t_{ch}	Characteristic minimum evolution time
r_{PMC}	Particle mask correlation coefficient
Sh	Cross-covariance shift
$R_{12,\text{max}}$	Maximum collocation coefficient between channel 1 and 2 particle image
\tilde{R}_{12}	Threshold for collocation median values
<i>Subscripts</i>	
1	Spectral channel 1
2	Spectral channel 2

Section S.2. PITC algorithm

S.2.1 Alignment and spatial registration

We spatially register the two channel images using a bright field image of an alignment pattern (Negative 1951 wheel pattern resolution test target from Thorlabs, R3L1S4N). Example misaligned (initial) and aligned (final) versions of this test pattern are shown in Figure S.1. We used Matlab's function `imregister`, an iterative process that requires a pair of images, an image-similarity metric, an optimizer, and a transformation type. The metric defines the image similarity for evaluating the accuracy of the registration. The optimizer defines the methodology for minimizing or maximizing the similarity metric. We used Matlab's function `imconfig` to generate the optimizer and metric assuming multimodal image capture, as the brightness range in the two spectral channels are different. The transformation type used for the image alignment is specified as "rigid", which consists of translation (Δi , Δj), and rotation (α). We set the maximum iterations to 1000. The ROI coordinates and the transformation matrix generated in this alignment phase are then used to translate and rotate the Ch2 particle image to achieve spatial registration with Ch1. Using images of simulated particle patterns; we have verified that this alignment procedure results in registration with sub-pixel accuracy. Note, the image alignment and registration process will produce artifacts at the perimeter of the images, which are eliminated by trimming ~ 5 pixels from the image edges. This entire process needs to be performed only periodically as a part of the instrumentation calibration procedure.

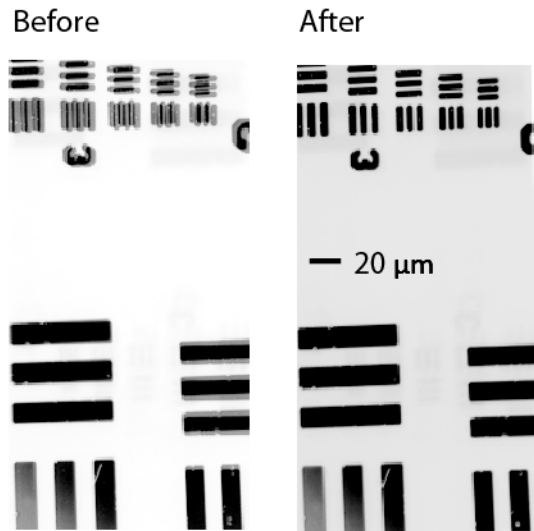


Figure S.1 Example of misaligned (initial) and aligned (final) bright-field images of two spectral channels recorded with a quad-view imager (Micro-Imager, Photometrics, Tucson, AZ), used here in dual-view mode. The images are plotted using Matlab's function, `imshowpair`, which displays the differences between two images. We used alpha blending to overlay the two spectral channel images before (left) and after (right) image registration. Note, alpha blending is the process of combining a translucent foreground color with a background color, which produces a new blended color. These test images were taken with a 20x objective with a numerical aperture of 0.5.

S.2.2 Particle tracking phase (Channel 1)

S.2.2.1. Micrometer-resolution Particle Image Velocimetry

We use measurements of spatially correlated particle motion (i.e., velocities averaged over finite subregions containing multiple particles) to guide our individual particle tracking algorithm. This correlated particle motion is the result of non-Brownian transport such as fluid flow or electrophoresis or both. Micro-PIV provides a robust and high-resolution method for determining such spatially correlated particle velocities.¹ Micro-PIV was developed specifically for microfluidic applications, and has been reviewed and described extensively.¹⁻³ The process limits particle tracking to particles near the focal plane of epifluorescence imaging.³ The standard process measures the x- and y-components of the velocity field in the imaging plane. For our micro-PIV analysis, we used 30 by 100 pixel interrogation regions with 50% overlap (for a total of 25 interrogation regions).^{4,5} Since the flows here were approximately steady, we typically averaged velocity information by ensemble averaging 50 correlation functions (each associated with an image pair) per velocity calculation.⁶ For the experimental data in Fig. 4 and Fig. 5, we ensemble averaged over 200 correlation functions.

S.2.2.2. Particle Mask Correlation method and Particle Characterization

Particle Mask Correlation (PMC)

PMC is performed in parallel with micro-PIV analysis. The PMC⁷ method identifies particle images and their coordinates by convolving raw images with a kernel “mask” made up of a two dimensional circularly symmetric Gaussian brightness pattern, I_m , expressed as follows:

$$I_m(x, y) = A \exp\left[-\frac{(x - x_o)^2 + (y - y_o)^2}{2\sigma_m^2}\right] \quad (2.1)$$

We set the peak brightness, A , to unity, but the value is arbitrary as we normalize cross-correlations between the image and particle mask (see Eq. 2.2). The mask standard deviation σ_m is chosen equal to or smaller than the radius of the smallest expected particle image radius in the image set. In our experiments, the particle brightness spans approximately 3 pixels, and so we set $\sigma_m = l_p$, where l_p is the pixel dimension in the object plane. The particle mask is scanned over the entire image plane and the normalized cross-covariance coefficient, r_{PMC} is calculated at each pixel location, (x_o, y_o) . The normalized cross-covariance coefficient between the particle mask centered at (x_o, y_o) and the image subregion of same size centered at (x_o, y_o) are computed as follows:

$$r_{PMC}(x_o, y_o) = \frac{\sum_{i=x_o-m/2}^{x_o+m/2} \sum_{j=y_o-n/2}^{y_o+n/2} (I(i, j) - \hat{I})(I_m(i, j) - \hat{I}_m)}{\sqrt{\sum_{i=x_o-m/2}^{x_o+m/2} \sum_{j=y_o-n/2}^{y_o+n/2} (I(i, j) - \hat{I})^2} \sqrt{\sum_{i=x_o-m/2}^{x_o+m/2} \sum_{j=y_o-n/2}^{y_o+n/2} (I_m(i, j) - \hat{I}_m)^2}} \quad (2.2)$$

In this study, we set the interrogation area, $n \times m$, to $8\sigma_m \times 8\sigma_m$. Here $I(i,j)$ is the brightness value of the particle image plane at (i,j) , and \hat{I} and \hat{I}_m are spatial averages of the brightness of the particle image plane and the particle mask image in the interrogation area, respectively.⁷ r_{PMC} varies between -1 to 1, depending on the degree of similarity between the brightness patterns. Pixels with high covariance coefficients indicate the presence of particles. Using a covariance threshold of 0.7 enables the PMC method to find all concentric convex brightness patterns of size of roughly $< 8 \sigma_m$.⁷ The calculated covariance coefficient plane is binarized using this threshold. For simplicity, we assign the pixel with the highest r_{PMC} value as the coordinate for the center of the particle, $(x_{p,l}, y_{p,l})$. As an approximation, we evaluate the particle image radius (geometrically projected into the object plane) as $r_{pi,l} = \sqrt{(gl_p)^2 / \pi}$, where g is the number of ‘unity’ pixels for a particle group in the binarized image, and l_p is the size of the pixel in the object space. While the cross-covariance was performed on raw particle images, the total, or integrated particle intensity, $I_{p,l}$, is estimated by summing the background corrected intensity of a $4r_{pi,l} \times 4r_{pi,l}$ subregion centered at the particle center $(x_{p,l}, y_{p,l})$. The corrected images are evaluated as follows:

$$I_c = \frac{I_{raw} - I_{bg}}{I_{flat}} . \quad (2.3)$$

The background of the raw image, I_{bg} is obtained by filtering the original image with a median filter of size $10\sigma_m \times 10\sigma_m$. The flatfield, I_{flat} , is obtained by imaging the microchannel filled with uniform concentration of dyes (1 μ M AF488 and 1 μ M AF647) which are processed with a median filter of size $10\sigma_m \times 10\sigma_m$.

Particle characterization (PC)

The PC method can significantly improve the accuracy of particle localization and the estimates for particle image radius, r_{pi} and integrated particle image intensity, I_p . In this routine we use a two dimensional circularly symmetric Gaussian brightness pattern, I_p , to fit the particle brightness patterns in the corrected images (See Eq. 2.3)

$$I_p(x, y) = A \exp \left[- \frac{(x - x_p)^2 + (y - y_p)^2}{2r_{pi}^2} \right] + b \quad (2.4)$$

The Gaussian fitting is performed on an $8\sigma_m \times 8\sigma_m$ subregion bounding the particle. As a first guess, the routine uses the median intensity of the subregion for the background, b ; the highest pixel intensity minus the background for the amplitude, A ; and the simple estimates, described in the PMC-PC section of the main paper, for particle coordinates and particle image radius for x_p , y_p and r_{pi} . We used and recommend this fitting routine for more detailed cytometry-like data of particle populations, as show in Fig. 5 of main paper. For the simulated particle-to-particle binding assay data we present in Figures 3 and S.4, we disabled this Gaussian fitting algorithm step in order to save computational time.

To eliminate large aggregates and out-of-focus particles from analysis, we implemented size- and intensity-based threshold filters. For the particle-to-particle collocation analysis presented in this study (unless stated otherwise), we set the size-based threshold to eliminate particles with radii larger than the mean plus 2 times the standard deviation of the particle population in each image. The intensity-based threshold eliminated all features with intensity 3 times the standard deviation away from the mean of the particle population. The output parameters of these phase includes particle coordinates, $x_{p,l}$, $y_{p,l}$, particle image radius, $r_{pi,l}$, and integrated fluorescence intensity, I_p , for each background-corrected particle image in the image sequence. In the next PITC phase (KC-PTV), we correlate and match particles identities between consecutive images in order to track their motion in time.

S.2.2.3. Kalman filter and χ^2 -test enhanced Particle Tracking Velocimetry

For robust and accurate operation, we use a Kalman filter and χ^2 -test^{7,8} to track each unique particle over time and space. This method, KC-PTV, was developed by Etoh and Takehara for particle tracking velocimetry.^{7,9} KC-PTV was later adapted for microfluidics by incorporating micro-PIV.^{10,11} In KC-PTV, particle image data (here location and particle image radius) from the first time step ($t=0$) is used to predict the particle information in the next time step ($t=t+\Delta t$). The probability of two particle images belonging to the same particle identity is evaluated using a χ^2 -test which uses the image data as parameters. See work by Takehara and co-workers^{7,8} for more detailed information on implementation.

In this phase of our algorithm, we apply filters to the data which reject particle image motions which are significantly far from bounds determined by local micro-PIV velocity data and particle diffusion estimates. For example, we reject particle matches with apparent velocities, $\bar{v}_{p,a}$, which fail the following criteria: $5v_{diff} > |\bar{v}_{p,a} - \bar{v}_{PIV}(x_{p,l}, y_{p,l})|$. Here, $v_{diff} = \sqrt{4D_p/\Delta t}$, and $\bar{v}_{PIV}(i, j)$ is the drift velocity at the particle position $(x_{p,l}, y_{p,l})$ obtained from micro-PIV analysis. Output parameters from this phase, including particle identification number (ID), and the corresponding particle coordinates, $x_{p,l}(t)$, $y_{p,l}(t)$, particle image radius, $r_{pi,l}(t)$, and integrated background-corrected fluorescence intensity, $I_p(t)$, are stored for further processing.

S.2.3. Particle collocation phase from Channel 1 and 2 data

Our particle collocation approach begins by positioning a small $8\sigma_m \times 8\sigma_m$ subregion at the coordinates of each particle identified and tracked in Ch1. The algorithm then selects a $16\sigma_m \times 16\sigma_m$ subregion in Ch2 centered at the same coordinates. We limit the shifts in correlations so that the Ch1 subregion always completely overlaps the Ch2 subregion, and so we eliminate the known biases associated with cross-correlations of finite-sized correlation functions.^{4,5} For the collocation analysis, we evaluate the normalized cross-covariance as described by Eq. 2.2, but where we set I_m to the Ch1 subregion and set I to the Ch2 subregion. The parameter r_{PMC} is then interpreted as the degree of correlation in the position of the particle or particles detected in both Ch1 and Ch2, which we refer to as collocation coefficient, $R_{12}(x_o, y_o, t)$. $R_{12}(x_o, y_o, t)$ is evaluated for widow offsets of (x_o, y_o) equal to or less than a predefined minimum value, $Sh = (r_{p,1} + r_{p,2}) + (1/4)\min(r_{pi,1}, r_{pi,2})$. We initially assign the offset

(x_o, y_o) with the highest $R_{12}(x_o, y_o, t)$ value as the coordinate for the center of the Ch2 particle, $(x_{p,2}, y_{p,2})$. If the maximum coefficient, $R_{12,\max}$, is below 0.6, we conclude that no particles are present in Ch2 subregion. For such a case, we set $r_{pi,2} = 0$ and estimate $I_{p,2}$ as the sum of the background corrected particle image intensity (Eq. 2.3) of a $4r_{pi,1} \times 4r_{pi,1}$ subregion centered at $(x_{p,1}, y_{p,1})$ in Ch2. If $R_{12,\max}$ is above 0.6, we conclude that there is a particle in the Ch2 subregion. To estimate the radius of the particle, we first binarize the collocation matrix and find the group of unity pixels associated with the Ch2 particle coordinates $(x_{p,1}, y_{p,1})$. We approximate the particle image radius as $r_{pi,2} = \sqrt{(gl_p)^2 / \pi}$. Particle radius is subsequently used to determine the Ch2 particle intensity, $I_{p,2}$, by summing the background corrected image intensity (Eq. 2.3) of a $4r_{pi,2} \times 4r_{pi,2}$ subregion centered at $(x_{p,2}, y_{p,2})$.

Recall that the particle characterization method (see Section S.2.2.2) can significantly improve the accuracy of particle localization, size and fluorescence characterization by using a sub-pixel resolution method. We implement the non-linear Gaussian fitting routine at this phase of the analysis for the data presented in Figure 4 and 5 of main paper.

References

1. Meinhart, C.D.; Wereley, S.T. and Santiago, J.G. *Experiments in Fluids*. **1999**, 27 (5), 414-419.
2. Santiago, J.G.; Wereley, S.T.; Meinhart, C.D.; Beebe, D.J. and Adrian, R.J. *Experiments in Fluids*. **1998**, 25 (4), 316-319.
3. Wereley, S.T. and Meinhart, C.D. *Annual Review of Fluid Mechanics*. **2010**, 42 (1), 557-576.
4. Adrian, R.J. and Westerweel, J. *Particle image velocimetry*. Cambridge University Press: 2010; Vol. 30.
5. Raffel, M.; Willert, C.E.; Wereley, S.T. and Kompenhans, J. *Particle Image Velocimetry—A Practical Guide*. 2 ed.; Springer Press: Heidelberg, 2007.
6. Meinhart, C.D.; Wereley, S.T. and Santiago, J.G. *Journal of Fluids Engineering*. **2000**, 122 (2), 285-289.
7. Takehara, K. and Etoh, G.T. *Journal of Visualization*. **1999**, 1 (3), 313-323.
8. Takehara, K.; Adrian, R. and Etoh, T. *Journal of the Visualization Society of Japan*. **1999**, 19 (Suppl 1), 319-322.
9. Takehara, K.; Adrian, R.J.; Etoh, G.T. and Christensen, K.T. *Experiments in Fluids*. **2000**, 29 (1), S034-S041.
10. Devasenathipathy, S.; Santiago, J.G. and Takehara, K. *Analytical Chemistry*. **2002**, 74 (15), 3704-3713.
11. Devasenathipathy, S.; Santiago, J.G.; Wereley, S.T.; Meinhart, C.D. and Takehara, K. *Experiments in Fluids*. **2003**, 34 (4), 504-514.

Section S.3. Effective diffusivity of a particle pair

The effective diffusivity of a pair of particles, D_{eff} , should scale with the standard deviation distance between two particles as follows:

$$\Delta r = r_2 - r_1 \sim \sqrt{D_{eff}} . \quad (3.1)$$

We assume that particle 1 and particle 2 positions r_1 and r_2 are statistically independent, and estimate a time average of their convolution as

$$\langle r_1 r_2 \rangle = 0 , \quad (3.2)$$

so the time averaged distance between them reduces to:

$$\langle (r_2 - r_1)^2 \rangle = \langle r_1^2 - r_1 r_2 + r_2^2 \rangle = \langle r_1^2 \rangle + \langle r_2^2 \rangle \sim D_{p1} + D_{p2} , \quad (3.3)$$

where D_{p1} and D_{p2} are respectively the diffusivities of particles 1 and 2. Very closely spaced particles may in fact exhibit a modified effective diffusivity, but we here offer this simple analysis to estimate statistics associated with particles diffusing away from each other.

Section S.4. 2D nearest neighbor model for randomly distributed particles

Let $w(r)dr$ denote the probability that the nearest neighbor to a particle occurs between r and $r+dr$. This probability must be equal to the probability that no particles exist interior to r times the probability that a particle does exist between r and $r+dr$. Therefore, the function $w(r)$ must satisfy the relation:

$$w(r) = \left[1 - \int_0^r w(r)dr \right] 2\pi r \eta \quad (4.1)$$

where η denotes the average number of particles per unit area. From Eq. 1 we can write

$$\frac{d}{dr} \left[\frac{w(r)}{2\pi r \eta} \right] = -2\pi r \eta \frac{w(r)}{2\pi r \eta} \quad (4.2)$$

Hence, the required law of distribution of the nearest neighbor becomes

$$w(r) = \exp(-\pi r^2 \eta) 2\pi r \eta \quad (4.3)$$

since, according to Eq. 4.1,

$$w(r) \rightarrow 2\pi r \eta \text{ as } r \rightarrow 0. \quad (4.4)$$

By definition, the average distance between particles with distribution $w(r)$ is

$$L_{IP} = \int_0^{\infty} r w(r) dr. \quad (4.5)$$

Combining Eq. 4.3 and 4.5, L_{IP} becomes

$$L_{IP} = \int_0^{\infty} \exp(-\pi r^2 \eta) 2\pi r^2 \eta dr. \quad (4.6)$$

After some basic reductions, we arrive to:

$$L_{IP} = \left(\frac{1}{\pi \eta} \right)^{1/2} \int_0^{\infty} \exp(-x) (x)^{1/2} dx \quad (4.7)$$

$$L_{IP} = \frac{1}{\sqrt{\pi \eta}} \Gamma\left(\frac{3}{2}\right) \quad (4.8)$$

Substituting for $\Gamma(3/2)$, we find

$$L_{IP} = 0.5 \eta^{-1/2}. \quad (4.9)$$

Section S.5. Influence of image SNR and particle density on particle tracking accuracy

Figure S.2 describes the influence of image signal-to-noise ratio (SNR) and particle density on the accuracy of our particle tracking algorithm, as determined using our Monte Carlo simulation images. Shown are histograms of tracked particle times in units of frames (the number of frames/images over which individual particles were successfully tracked) as a function of SNR and L_{IP}/L_{ch} .

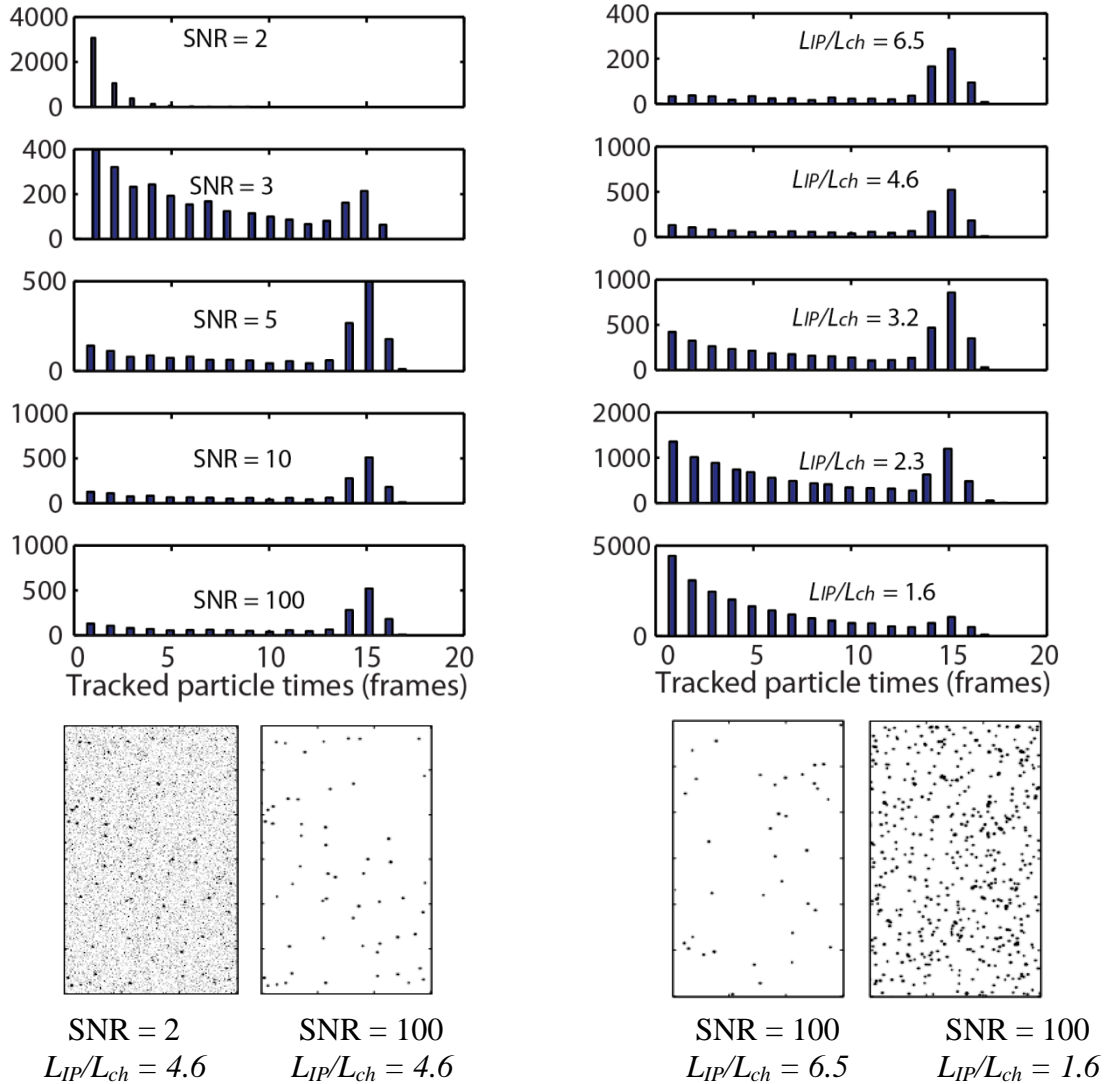


Figure S.2. Histogram of the number of particles that were tracked for 1 to 20 frames. Left: Simulated particle density was set to 100 particles/domain ($L_{IP}/L_{ch} = 4.6$). The PMC method relies on brightness patterns for identification of particles. When SNR is too low ($SNR \leq 6$), the brightness patterns are distorted and particles are not easily identified. For SNR of 5 or above, over 95% of particles are tracked for 10 s or longer. Right: SNR for Monte Carlo simulated images were set to 100. PMC method fails if particle brightness pattern is overly affected by neighboring particles and Kalman filter and χ^2 test will fail as trajectories of closely spaced particles become indistinguishable. As the inter-particle distance decreases, the particles can be tracked successfully for progressively shorter times as they are lost due to particle crowding. For $L_{IP}/L_{ch} \leq 3.2$ large fractions of these particles are tracked for shorter times than that required for collocation (i.e., the minimum evolution time, t_{ch} , defined in Eq. 2 of main paper).

Section S.6. Limit of detection of PITC method

To study the limit of detection (LOD) of our method in the absence of bound particles and to quantify false positive rates in negative controls, we performed collocation on image sets with 0% simulated bound particle fraction (Fig. S.3). The total number of 1 μm diameter particles in each image from the Monte Carlo simulation is 100 (with a mean inter-particle distance of roughly 14 μm). At image SNR = 100, the PITC algorithm found that bound particle doublets made up 0.9%, 0.6%, and 0.25% of the total particles with collocation threshold values of 0.6, 0.7 and 0.8, respectively. False positive collocation detections occur in the negative control case due to failure of the particle intensity threshold filter we implemented in the collocation phase. This intensity based threshold relies on the intensity distribution of true positive particle matches in Ch2. Since there are no true positive matches in the negative control case, the intensity distribution obtained this way is not a true representation of the Ch2 particle intensities. These bound fractions, therefore, represent the limit of detection (LOD) of our method in the absence of a priori Ch2 particle intensity calibration. To improve the LOD, we recommend the evaluation of particle intensities in Ch2 using the PMC-PC method. The calibrated intensity distribution can then be used to filter particle matches in the collocation phase. After we performed a simple calibration of Ch2 particles, the PITC algorithm detected 0% bound fractions for all collocation thresholds in the negative control case.

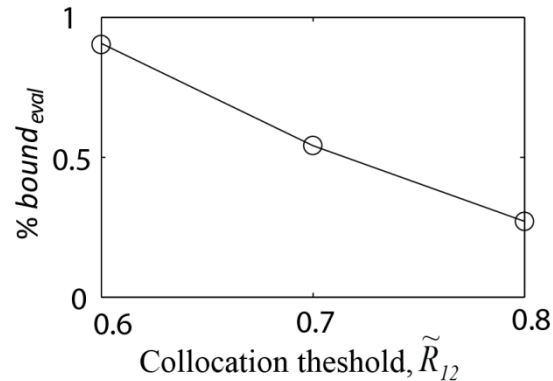


Figure S.3. Limit of detection of PITC collocation in the absence of particle intensity calibration. Using three collocation threshold values, PITC detected 0.9%, 0.5% and 0.3% false positive bound fraction in the simulated image sets. The false positive bound fraction is reduced to 0% for all \tilde{R}_{12} , when calibrated Ch2 particle intensity distribution is used as the basis of the intensity-based filter in the collocation phase.

Section S.7 Influence of particle density on collocation performance

In Figure S.4, we analyze the influence of particle density on collocation performance by comparing the inter-particle distance, L_{IP} , to the characteristic distance that two randomly aligned particles must separate for the algorithm to consider them unbound, L_{ch} (Eq. 1 of main paper). Here we also examine the influence of monitoring time, t_m on collocation by comparing t_m to the minimum elution time, t_{ch} (Eq. 2 of main paper), the characteristic time it takes two randomly bound particles to separate by L_{ch} . Fig. S.4 shows the ratio between the evaluated and simulated bound fraction as a function of L_{IP}/L_{ch} and t_m/t_{ch} , using two collocation thresholds $\tilde{R}_{12} = 0.6, 0.7$. In a single instance in time, the collocation algorithm cannot differentiate between random and deterministic particle interactions. When particle densities are low (high L_{IP}/L_{ch}), the random particle-particle interactions are rare, and the bound fractions detected by PITC converge to the simulated values for all t_m and \tilde{R}_{12} . When high particles densities (low L_{IP}/L_{ch}) yield frequent random particle-particle interactions, the bound particle fractions for short observation times are over-predicted as expected. For example, for $L_{IP}/L_{ch} = 1.6$ and a collocation threshold of $\tilde{R}_{12} = 0.6$, the PITC algorithm detects ~ 6.2 times the simulated bound particle events for the shortest monitoring time ($t_m/t_{ch} = 0.77$). Using a more conservative collocation threshold, $\tilde{R}_{12} = 0.7$, this error reduces to ~ 3.2 times the simulated fraction. For both values of \tilde{R}_{12} , increasing monitoring time improves collocation accuracy. When we increase the monitoring time to more than four times the evolution time of particle pairs ($t_m/t_{ch} > 3.87$), the PITC algorithm detects ~ 1.5 times the simulated fraction at a challenging value of $L_{IP}/L_{ch} = 1.6$ (using $\tilde{R}_{12} = 0.7$).

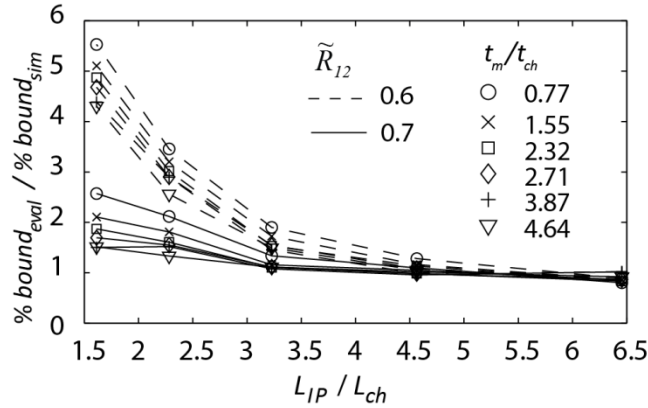


Figure S.4. Accuracy of particle hybrid count as a function of particle density, monitoring time, and collocation threshold. The simulated fraction of bound particles was set to 3%, and the image SNR to 100. For all collocation thresholds, as the inter-particle distance decreases, the frequency of random particle-particle interaction increase. As a result, the algorithm overestimates the bound particle fraction. While the accuracy of collocation improves by increasing the monitoring time, t_m , and increasing collocation threshold, \tilde{R}_{12} from 0.6 to 0.7, the error in the detected fraction for $L_{IP}/L_{ch} < 3$ is still significant. At $L_{IP}/L_{ch} = 1.6$, $\tilde{R}_{12} = 0.7$, and $t_m/t_{ch} = 3.87$, PITC detects 4.5% bound. Using the same algorithm settings on image sets with lower particle density, PITC detects 3.23%, 2.87 % and 3.06% bound particle fractions at L_{IP}/L_{ch} of 3.2, 4.6 and 6.5, respectively.

While this trend suggests that increasing monitoring time leads to improved collocation accuracy, recall from Fig S.2 at high particle densities, the monitoring time is severely limited by the short L_{IP} . Based on these results we recommend using particle densities which yield approximately $L_{IP}/L_{ch} > 3$, and collocation threshold of $\tilde{R}_{12} = 0.7$, but note that low SNR images will likely require a slightly lower value of 0.6 or 0.65. Finally, for all cases, we conclude that increasing monitoring time increases collocation certainty. In general, we recommend monitoring times of 2 times the minimum evolution time, t_{ch} , or higher. For our recommend value of $\tilde{R}_{12} = 0.7$ and a value of $t_m/t_{ch} = 3.87$ PITC predictions are within $\sim 10\%$ or less for $SNR = 100$, for the case of only 3% particles bound (bound fraction is estimated between 2.7% - 3.3% for $L_{IP}/L_{ch} > 3$).

Section S.8. DNA induced bead-to-bead binding assay

We demonstrate our assay by detecting the presence of target DNA by collocation of fluorescent beads bound to this target. Each bead had a unique spectral signature (red and green emission) and each was functionalized with unique DNA probe complementary to a portion of the target. When these probes hybridize to the target DNA, the two beads form a two-color doublet (Fig. S.5) The final bead solution contains at least three bead populations, red singlets, green singlets, and red-green bead doublets. We load the bead suspension onto a microfluidic chip (Fig. S.6) and image the beads as they traverse through the interrogation region. The beads used in this assay were carboxylate modified, (negatively charged at the operating pH of 8), so they electrophorese in the presence of an applied electric field. The beads were suspended freely in solution, so that we can leverage Brownian motion to separate randomly colocated beads, and so distinguish these from those which are deterministically bound via a DNA target.

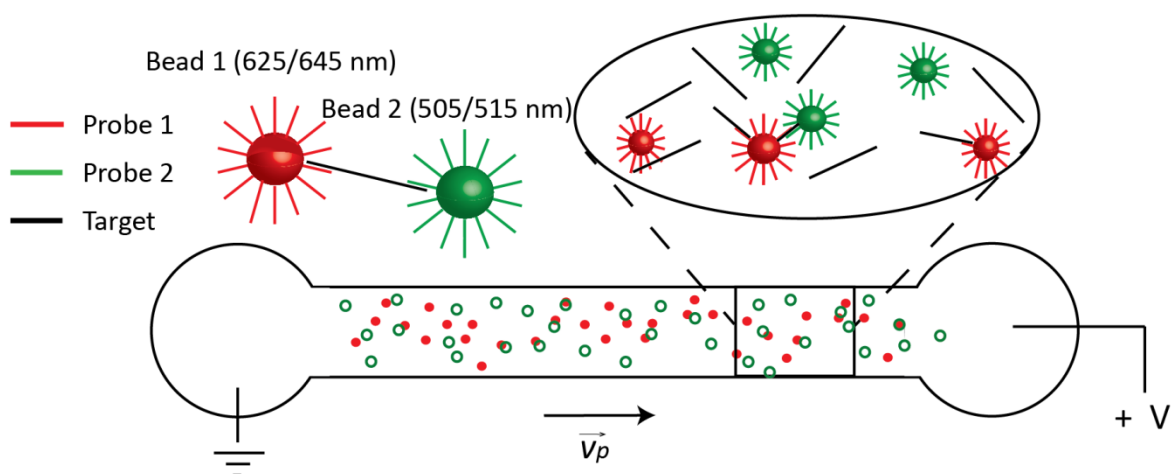


Figure S.5. Collocation particle imaging for DNA detection. A solution containing red and green beads was mixed with target DNA in a hybridization buffer. Bead doublet formed when Probe 1 on red fluorescence bead (Bead 1) and Probe 2 on green fluorescence bead (Bead 2) are hybridized to the target DNA sequence. The bead-DNA mixture was electrophoresed in a channel with a transparent top wall and visualized using a microscope equipped with a dual-view system and high-sensitivity CCD camera.

Section S.9. List of fluorescent beads and DNA sequences

Bead 1:

FluoSpheres® microspheres (Molecular Probes, Life Technologies)

Label (Ex/Em): Yellow-green (505/515 nm)

Catalog number: F8823

Nominal bead diameter: 1.0 µm

Coupling surface: Carboxylate

Solids: 2%

DNA probe (desalted):

5'- Amino Modifier C12- CACAAAGTGGTAAGCGCCCTC

Bead 2:

FluoSpheres® microspheres (Molecular Probes, Life Technologies)

Label (Ex/Em): Crimson-fluorescent (625/645 nm)

Catalog number: F8816

Nominal bead diameter: 1.0 µm

Coupling surface: Carboxylate

Solids: 2%

DNA probe (desalted):

5'- Amino Modifier C12 – CGGATTGGAGTCTGCAACTCG

The target DNA used was as follows:

DNA target (PAGE purified):

AAACGAGTTGCAGACTCCAATCCGAAAAGAAGTAGGTAGCTTAACCTTCGGGAGGG
CGCTTACCACTTTGTGTTT

DNA sequences

The desalted DNA probes and PAGE purified DNA targets were purchased from Integrated DNA Technologies (IDT, Coralville, IA)

Immobilization

Beads were functionalized with Amine modified DNA probes by Radix Biosolutions (Georgetown, TX), and suspended in Tris-EDTA, pH 8 at 2% solids.

Section S.10. Chip schematic and loading protocol

The buffered bead suspension contained 20 mM Tris, 10 mM hydrochloric acid, HCl, 0.08% Triton X-100, 50 mM sodium chloride, NaCl, 10 nM target DNA, and 3×10^8 beads/mL of each color. The solution was pressure loaded into a poly(methyl methacrylate) (PMMA) microfluidic chip of dimensions 2 mm x 150 μ m x 10 cm (total length). End-channel reservoirs and one mid-channel reservoir were filled with approximately the same volume of aqueous buffer solution (1 M Tris, 500 mM HCl) in attempt equalize hydrostatic pressure and minimize pressure driven flow. To reduce unwanted pressure-driven flows in the channels, we used pluronic-F127 as a phase change material to seal off the buffering well.¹ Our mixture of pluronic-F127 is a liquid at low temperature and solidifies into a gel at room temperature.²

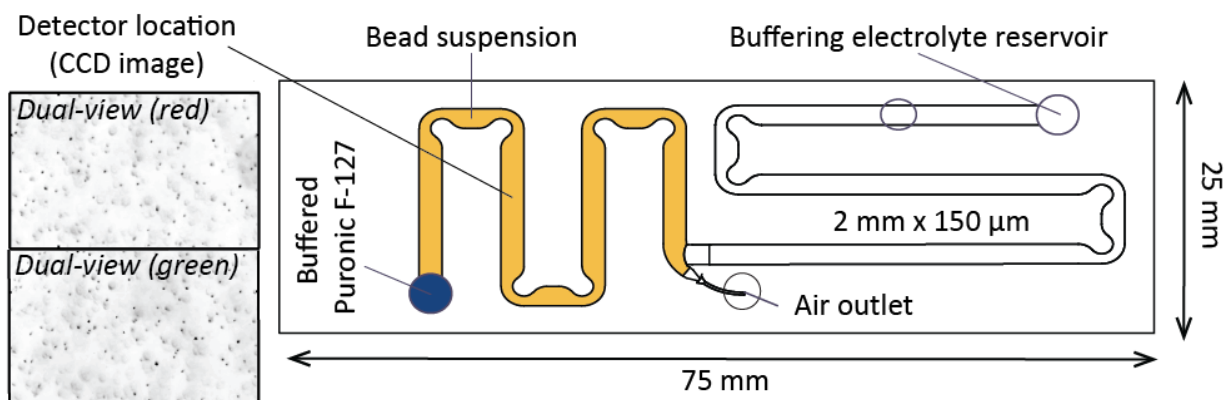


Figure S.6. Fluidic channel architecture and loading protocol used in demonstration of particle imaging, tracking and collocation method. The microfluidic fluidic chip was loaded with the buffered bead suspension. The output well was filled with 50 μ l of 1 M Tris-HCl (pH 8) buffer. The loading well was filled with the same buffer containing 25% Pluronic F-127 solution in order to reduce pressure driven flow. Platinum electrodes were placed in the loading and output well and electrophoresis was initiated by applying 100 μ A across the microchannel. In a typical experiment, we record 200 chromatically separated particle images at a frequency of 1Hz. During this time, order 1,000-10,000 unique beads traverse through the field of view.

Reference

1. Marshall, L.A., Rogacs, A., Santiago, J.G., An Injection Molded Microchip for Nucleic Acid Purification from 25 Microliter Samples using Isotachopheresis, *under review*.
2. Vadnere, M., G. Amidon, et al. (1984). "Thermodynamic studies on the gel-sol transition of some pluronic polyols." *International Journal of Pharmaceutics* 22(2-3): 207-218.